*FUDMA Journal of Sciences (FJS)*
*ISSN online: 2616-1370*
*ISSN print: 2645 - 2944*
*Vol. 10 No. 24, December, 2026, pp 232 – 239*
*DOI:* https://doi.org/10.33003/fjs-2026-1024-6338

# Field-Based Biomass and Carbon Stock Estimation and Landsat-Derived Spatial Patterns in Tula Highland, Gombe State, Nigeria

***[1]Yuguda Usman Abubakar, [2]Moruff Gbolagade Saka and [2]Ephraim Edward Dishan**

[1]Department of Plant Sciences, Gombe State University, Gombe, Gombe State, Nigeria.
[2]Department of Forestry and Wildlife Management, Modibbo Adama University, Yola, Adamawa State, Nigeria.

*Corresponding authors' email: uayuguda@gsu.edu.ng
ORCID iD: https://orcid.org/0000-0003-3005-3130

**Received:** 27 Oct. 2026
**Accepted:** 10 Nov. 2026
**Published:** 14 Nov. 2026

**ABSTRACT**
Highland vegetation is poorly represented in Nigeria's carbon accounting. We estimated aboveground (AGB) and belowground biomass (BGB) and biomass carbon stocks in Tula Highland, Gombe State, and examined their relationship with Landsat-derived vegetation indices. Woody vegetation was inventoried in 13 one-hectare plots, spaced 1 km apart, between February and June 2025. AGB was estimated with allometric equations, BGB with a fixed root-to-shoot ratio of 0.26, and carbon with a fraction of 0.47; litter was reported separately. Landsat 8 OLI imagery for 2020–2024 was used to compute NDVI, SAVI and ARVI. Mean densities were 23.55 Mg ha$^{-1}$ for AGB (95% CI 10.27–36.82) and 6.12 Mg ha$^{-1}$ for BGB, a combined 29.67 Mg ha$^{-1}$ (13.95 Mg C ha$^{-1}$), with large variation among plots (0.18–108.62 Mg ha$^{-1}$). Summed over the plots, AGB and BGB were 306.14 and 79.60 Mg (181.29 Mg C). Because BGB is a fixed fraction of AGB, it carries no independent information; a ratio of 0.56 would raise mean total biomass to 36.74 Mg ha$^{-1}$. A three-index linear model gave an adjusted $R^2$ of 0.986 (AIC = 173.93) for the calibration plots, but the small sample, near-collinear indices and lack of independent validation limit confidence in spatial predictions. Model-derived mean AGB rose by 16.99% between 2020 and 2024; this reflects spectral change, not measured biomass accumulation or carbon sequestration. The results are a preliminary baseline and show the need for more plots, repeated inventories and formal uncertainty assessment.

**Keywords:** Aboveground Biomass, Belowground Biomass, Carbon Stock, Landsat 8, Vegetation Indices, Tula Highland

## INTRODUCTION

Aboveground biomass is an Essential Climate Variable (GCOS, 2016) and a basic input to national greenhouse gas inventories and REDD+ reporting (Bos et al., 2019; Herold et al., 2019). Uncertainty in biomass estimates remains a major constraint on carbon accounting (Kumar & Mutanga, 2017; Temesgen et al., 2015). Belowground biomass is measured less often than aboveground biomass, although roots may make up 10–40% of total biomass depending on species composition and site conditions (Mokany et al., 2006). Montane and highland vegetation is climate-sensitive and data-poor, and it is rarely represented in biomass inventories. Nigeria's Climate Change Act of 2021 created the National Council on Climate Change and a legal basis for carbon markets (Ajayi, 2026; PwC, 2023), which increases the demand for biomass and carbon data. Such data remain scarce for non-forest woody and highland vegetation. Tula Highland in Gombe State combines rock outcrops, mixed montane–savanna flora and smallholder land use (Jimoh et al., 2022; Yilangai et al., 2023), and its biomass has not been quantified. Satellite vegetation indices are widely used to extend plot measurements over larger areas (Kumar & Mutanga, 2017). Relationships calibrated in closed-canopy forest or lowland savanna do not transfer readily to rocky highland terrain, where bare rock and soil contribute much of the pixel signal, so Tula Highland needs its own calibration. Three indices were considered here. NDVI is simple but sensitive to soil background where canopy cover is sparse (Huete, 1988). SAVI includes a soil-adjustment factor (Huete, 1988), and ARVI uses the blue band to reduce atmospheric effects (Kaufman & Tanré, 1992). The indices may carry complementary information, but they are algebraically related and highly correlated, which complicates regression.

Two limitations shape the interpretation of this kind of work. First, a standing carbon stock is not carbon sequestration: a stock is the amount stored at one time, whereas sequestration is a net annual flux that requires repeated measurement. Second, a single-date field inventory cannot validate multi-year change in image-derived estimates, because spectral change may reflect phenology, herbaceous growth, or atmospheric and compositing effects rather than change in woody biomass. This study therefore treats the field inventory as the measured quantity and the satellite results as exploratory.

This study aimed to estimate aboveground and belowground biomass and associated carbon stocks in Tula Highland, Gombe State, and evaluate the potential of Landsat-derived vegetation indices for spatial biomass estimation.

## MATERIALS AND METHODS

### Study Area

Tula Highland lies in Kaltungo Local Government Area, Gombe State, north-eastern Nigeria (Figure 1), between latitudes 9°48′N and 9°54′N and longitudes 11°25′E and 11°31′E. It covers approximately 6,381 ha at an elevation of 645 m above sea level. The climate is tropical savanna (Köppen classification; Jimoh et al., 2022). The vegetation is a light, discontinuous canopy with scattered shrubs and sparse grass cover, which becomes open and largely grassless where rock outcrops dominate (Jimoh et al., 2022). Woody species

of highest structural importance in the plots were *Guiera senegalensis*, *Parkia biglobosa*, *Khaya senegalensis*, *Lantana camara*, *Balanites aegyptiaca* and *Raphia sudanica*; *Ficus thonningii* and *Vitex doniana* are also characteristic of the highland, and *Panicum maximum* occurs in the grass layer (Jimoh et al., 2022). Local microclimates support relatively high floristic diversity (Yilangai et al., 2023), and the highland protects watersheds and supplies fuelwood, fodder and non-timber products to nearby communities.

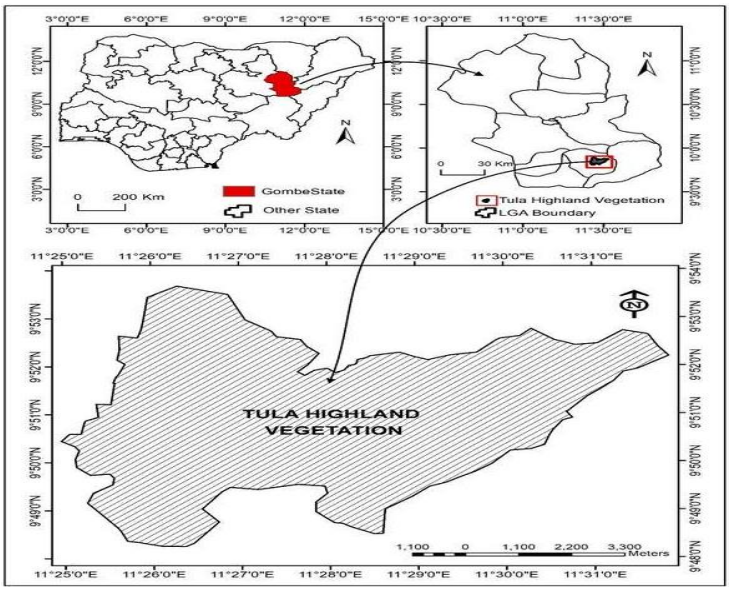



Figure 1: Location and extent of Tula Highland vegetation, Kaltungo Local Government Area, Gombe State, Nigeria (source: GIS Laboratory, Gombe State University)

**Plot Design and Field Measurements**

Thirteen plots of 100 m × 100 m (1 ha) were established at fixed, equal intervals in a systematic design (Ravindranath & Ostwald, 2008), about 0.2% of the highland area. The number of plots followed minimum sampling-intensity recommendations for areas of low to moderate tree density (Rügnitz et al., 2009). Plots were spaced 1 km apart and measured from February to June 2025. Each plot covers about 11 Landsat 8 pixels. Within each plot, four 20 m × 20 m subplots at the corners were used for tree enumeration, 5 m × 5 m subplots nested within them for shrubs, and a 1 m × 1 m subplot for litter (Bordoloi et al., 2021).

To convert biomass recorded within nested subplots to standardised per-hectare densities (Mg ha$^{-1}$), stratum-specific expansion factors (EF) were applied based on the sampled surface area within each 1.0-ha (10,000 m²) macro-plot (Bordoloi et al., 2021). For mature trees, the four 20 m × 20 m corner subplots sampled a cumulative area of 1,600 m² (0.16 ha) per plot, so tree biomass was scaled to one hectare using an expansion factor of

$EF_{tree}$ = 10,000 m² / 1,600 m² = 6.25:

$AGB_{trees}$ (Mg ha$^{-1}$) = ($\Sigma$ $AGB_{tree}$ (kg) × 6.25) / 1,000 (1)

For shrubs and saplings, the four 5 m × 5 m nested subplots sampled a total area of 100 m² (0.01 ha) per plot, and shrub biomass was expanded to one hectare using

$EF_{shrub}$ = 10,000 m² / 100 m² = 100.0:

$AGB_{shrubs}$ (Mg ha$^{-1}$) = ($\Sigma$ $AGB_{shrub}$ (kg) × 100.0) / 1,000 (2)

For surface litter necromass, four 0.5 m × 0.5 m quadrats sampled a cumulative area of 1.0 m² (0.0001 ha) per plot, and oven-dry litter mass was scaled to one hectare using

$EF_{litter}$ = 10,000 m² / 1.0 m² = 10,000:

Litter necromass (Mg ha$^{-1}$) = ($W_{dry}$ (g m$^{-2}$) × 10,000) / 1,000,000 = $W_{dry}$ (g m$^{-2}$) × 0.01 (3)

Diameter at breast height (DBH, measured at 1.3 m) and total height were recorded for all woody individuals. Trees with stems of 10 cm DBH or more, and shrubs and saplings with stems of 1–9 cm DBH. In shrubs and small trees, diameter was measured near the base or at the point of branching, whichever was more representative of the stem. Height was measured with a clinometer.

Litter was collected from 0.5 m × 0.5 m quadrats placed within the 1 m × 1 m subplots (Asrat et al., 2018). The material comprised fine necromass, dead wood less than 5 cm in diameter or 50 cm in length, non-decomposed plant material, unburned leaves and branches, and partly decomposed litter. Samples were oven-dried and weighed. Litter is reported separately and is not included in the AGB, BGB or carbon totals.

**Biomass and Carbon Estimation**

Tree AGB was estimated from DBH and height with Equation 4, using the coefficients of the multi-species savanna equation of Henry et al. (2009) (see also Chave et al., 2014): $a$ = 0.051 and $b$ = 0.930, for AGB in kg. Shrub AGB was estimated from stem diameter with Equation 5 (Conti et al., 2019), with $a$ = 0.0568 and $b$ = 2.584. The equation of Conti et al. (2019) was used because it is a global shrub model.

$AGB = a \times (DBH^2 \times H)^b$ (4)

Where DBH is diameter at breast height (cm) and H is total tree height (m).

$AGB = a \times D^b$ (5)

Where D is shrub stem diameter (cm).

Aboveground carbon was calculated with a carbon fraction of 0.47 (IPCC, 2006, 2019):

$C_{AGB} = AGB \times 0.47$ (6)

Litter biomass (LB, kg ha$^{-1}$) was calculated from the dry mass collected per unit quadrat area:

$LB = (W / A) \times 10$ (7)

Where W is dry mass of litter (g) and A is quadrat area (m²); the factor 10 converts g $m^{-2}$ to kg $ha^{-1}$.

BGB was estimated as a fixed fraction of AGB for trees and shrubs (Equation 8), using a root-to-shoot ratio (*R*) of 0.26 (IPCC, 2006; Mokany et al., 2006; Ma et al., 2021). Because BGB is then a deterministic function of AGB, it carries no independent belowground information. The ratio is lower than some IPCC defaults for dry tropical vegetation, and the effect of a higher value is shown in the Results. Belowground carbon was derived with the same carbon fraction (Equation 9). Carbon was converted to $CO_2$-equivalent by multiplying by 44/12.

$$BGB = AGB \times R \quad (8)$$

$$C_{BGB} = BGB \times 0.47 \quad (9)$$

**Remote Sensing Data**

Landsat 8 Operational Land Imager (OLI) scenes for 2020–2024 (30 m spatial resolution) were downloaded from the USGS EarthExplorer archive and used to derive NDVI, ARVI and SAVI datasets to assess vegetation conditions. The imagery was referenced to WRS-2 Path/Row 186/053, and the vegetation-index rasters were clipped to the study-area boundary using the Extract by Mask tool in ArcGIS. The original scene-level metadata and processing records were unavailable; exact acquisition dates, annual scene counts, product processing levels, cloud-cover thresholds and cloud-masking procedures therefore could not be independently verified. Bands were stacked in ArcMap, converted from digital numbers to top-of-atmosphere reflectance with scene metadata, and corrected for atmospheric scattering by dark object subtraction. Images were processed at the Zonal Advanced Space Technology Applications Laboratory, National Centre for Remote Sensing, Federal University Kashere, Gombe State, Nigeria. Annual mean temperature and total precipitation for 2020–2024 were obtained from the Nigerian Meteorological Agency (NIMET).

NDVI (Rouse et al., 1974; Tucker, 1979), SAVI (Huete, 1988) and ARVI (Kaufman & Tanré, 1992) were computed for each pixel:

$$NDVI = (NIR - RED) / (NIR + RED) \quad (10)$$

$$SAVI = [(NIR - RED) \times (1 + L)] / (NIR + RED + L) \quad (11)$$

$$ARVI = [NIR - (RED - \gamma\,(RED - BLUE))] / [NIR + (RED - \gamma\,(RED - BLUE))] \quad (12)$$

Where NIR, RED and BLUE are reflectance in the near-infrared, red and blue bands, L is the soil-adjustment factor ($L = 0.5$) and $\gamma$ is the atmospheric correction coefficient ($\gamma = 1$). For each index, annual maximum-value composites were produced by selecting the highest value recorded for each pixel in a year, which reduces the effects of cloud and seasonal fluctuation. Five-year mean vegetation-index values (2020–2024) were paired with the 2025 field inventory data for biomass calibration. The imagery was used to represent longer-term spectral conditions rather than contemporaneous ground observations, and the temporal mismatch was recognised as a potential source of uncertainty in the biomass–vegetation index relationships.

**Statistical Analysis**

Candidate models were multiple linear regressions of plot AGB on all seven non-empty combinations of NDVI, SAVI and ARVI, fitted by ordinary least squares. Each combination was fitted to AGB, log-transformed AGB and inverse-transformed AGB, giving 21 models. Models were ranked with Akaike's information criterion ($AIC = 2k - 2\ln L$, where k is the number of estimated parameters and L the maximised likelihood). AIC values were compared only within a response form, because likelihoods defined on different response scales are not comparable. Models with $\Delta AIC$ below 2 were considered to have similar support (Burnham & Anderson, 2002). Prediction uncertainty was assessed by Monte Carlo simulation with 500 runs (Chave et al., 2004; Yanai et al., 2010). The coefficient of variation (CV) of the simulated predictions indicates the stability of the model under the simulated parameter variation. It does not measure predictive accuracy. The selected equation was applied to the annual composites to produce AGB maps for 2020–2024. Climate and spectral rasters were co-registered to a common grid, and zonal statistics were calculated over the study polygon (Tomlin, 1990). Pearson correlations between annual mean indices and annual climate used n = 5 years.

## RESULTS AND DISCUSSION

**Biomass and Carbon Stocks**

Plot values are given in Table 1 and summary statistics in Table 2. Mean AGB across the 13 plots was 23.55 Mg $ha^{-1}$ (SD 21.97; 95% confidence interval 10.27–36.82) and mean BGB was 6.12 Mg $ha^{-1}$ (SD 5.71), giving a mean total biomass of 29.67 Mg $ha^{-1}$ (SD 27.68; 95% CI 12.94–46.40). Mean carbon density was 13.95 Mg C $ha^{-1}$ (11.07 aboveground and 2.88 belowground), equivalent to 51.18 Mg $CO_2$-e $ha^{-1}$. Summed over the 13 sampled hectares, AGB was 306.14 Mg and BGB 79.60 Mg, holding 143.88 and 37.41 Mg C respectively (181.29 Mg C, or 665.35 Mg $CO_2$-e, in total). These totals refer to the sampled plots only and are not densities or estimates for the whole highland. Mean litter biomass was 9,050.83 ± 997.03 kg $ha^{-1}$ (SD 4.15 and SE 1.31) and is not included in the totals.

**Table 1: Aboveground and Belowground Biomass and Carbon Stocks in the 13 Plots, Tula Highland. Plot Values are Per Hectare (Mg $ha^{-1}$)**

| Plot | AGB | AGC | AGC as $CO_2$-e | BGB | BGC | BGC as $CO_2$-e | Total biomass |
|---|---|---|---|---|---|---|---|
| TH 1 | 21.20 | 9.97 | 36.57 | 5.51 | 2.59 | 9.51 | 26.72 |
| TH 2 | 18.31 | 8.61 | 31.58 | 4.76 | 2.24 | 8.21 | 23.07 |
| TH 3 | 12.79 | 6.01 | 22.06 | 3.32 | 1.56 | 5.73 | 16.11 |
| TH 4 | 36.47 | 17.14 | 62.91 | 9.48 | 4.46 | 16.36 | 45.95 |
| TH 5 | 26.31 | 12.37 | 45.38 | 6.84 | 3.22 | 11.80 | 33.15 |
| TH 6 | 25.60 | 12.03 | 44.17 | 6.66 | 3.13 | 11.48 | 32.26 |
| TH 7 | 0.91 | 0.43 | 1.56 | 0.24 | 0.11 | 0.41 | 1.14 |
| TH 8 | 33.88 | 15.92 | 58.44 | 8.81 | 4.14 | 15.20 | 42.69 |
| TH 9 | 19.73 | 9.27 | 34.04 | 5.13 | 2.41 | 8.85 | 24.86 |
| TH 10 | 0.14 | 0.07 | 0.24 | 0.04 | 0.02 | 0.06 | 0.18 |
| TH 11 | 5.16 | 2.42 | 8.90 | 1.34 | 0.63 | 2.31 | 6.50 |
| TH 12 | 86.20 | 40.52 | 148.69 | 22.41 | 10.53 | 38.66 | 108.62 |

| Plot | AGB | AGC | AGC as $CO_2$-e | BGB | BGC | BGC as $CO_2$-e | Total biomass |
|---|---|---|---|---|---|---|---|
| TH 13 | 19.43 | 9.13 | 33.51 | 5.05 | 2.37 | 8.71 | 24.48 |
| Sum (Mg) | 306.14 | 143.88 | 528.06 | 79.60 | 37.41 | 137.29 | 385.73 |
| Mean (Mg ha$^{-1}$) | 23.55 | 11.07 | 40.62 | 6.12 | 2.88 | 10.56 | 29.67 |

AGB, aboveground biomass; AGC, aboveground carbon; BGB, belowground biomass; BGC, belowground carbon; $CO_2$-e, $CO_2$-equivalent. Sums and means were calculated from unrounded values and may differ slightly from the sums of the rounded entries.

**Table 2: Sums and Mean Densities of Biomass and Carbon across the 13 Plots**

| Quantity | Sum across 13 plots | Mean (per ha) | SD | 95% CI of mean |
|---|---|---|---|---|
| AGB | 306.14 Mg | 23.55 | 21.97 | 10.27–36.82 |
| AGC | 143.88 Mg C | 11.07 | 10.32 | 4.83–17.31 |
| BGB | 79.60 Mg | 6.12 | 5.71 | 2.67–9.57 |
| BGC | 37.41 Mg C | 2.88 | 2.68 | 1.26–4.50 |
| Total biomass | 385.73 Mg | 29.67 | 27.68 | 12.94–46.40 |
| Total carbon | 181.29 Mg C | 13.95 | 13.01 | 6.08–21.81 |
| Total $CO_2$-equivalent | 665.35 Mg $CO_2$-e | 51.18 | 47.74 | 22.33–80.03 |

Mean and SD are in Mg ha$^{-1}$ (carbon in Mg C ha$^{-1}$; $CO_2$-equivalent in Mg $CO_2$-e ha$^{-1}$). Confidence intervals use the t distribution with 12 degrees of freedom.

Biomass varied about 600-fold among plots, from 0.18 Mg ha$^{-1}$ (TH 10) to 108.62 Mg ha$^{-1}$ (TH 12), and the coefficient of variation was 93%. TH 12, where *Parkia biglobosa*, *Khaya senegalensis* and *Raphia sudanica* were structurally important, held 28% of the summed AGB. TH 10 and TH 7 (1.14 Mg ha$^{-1}$) were sparse, rock-dominated plots. The dense stand in TH 12 may reflect a moisture-favoured micro-site, but soil moisture and topography were not measured. The wide confidence interval shows that the 13-plot mean is an imprecise estimate for the highland.

Mean total biomass (29.67 Mg ha$^{-1}$) is lower than the shrub-savanna (45.29 Mg ha$^{-1}$) and riparian-forest (94.58 Mg ha$^{-1}$) values reported for the Sudan savanna of Benin (Chabi et al., 2016), although the upper limit of the present confidence interval (46.40 Mg ha$^{-1}$) reaches the shrub-savanna value. These are standing stocks. They do not show that the highland is removing $CO_2$ from the atmosphere, which would require repeated measurement of biomass change.

**Belowground Biomass**

BGB made up 20.6% of total biomass (79.60 of 385.73 Mg). This follows directly from the fixed ratio of 0.26 and is not a property of the vegetation. The spatial pattern of BGB therefore duplicates that of AGB, and BGB cannot be validated independently of it. Shallow, rocky soils often promote greater root allocation (Mokany et al., 2006; Ma et al., 2021), so a uniform ratio may underestimate belowground storage on exposed plots. Using R = 0.56, the IPCC (2006) default for tropical dry forest with AGB below 125 Mg ha$^{-1}$, would raise mean BGB from 6.12 to 13.19 Mg ha$^{-1}$ and mean total biomass from 29.67 to 36.74 Mg ha$^{-1}$. Excavation-based root allometry for dominant highland species is needed to narrow this uncertainty.

**Vegetation Indices and Climate**

Mean annual NDVI, SAVI and ARVI over 2020–2024 were 0.22, 0.33 and 0.14, low values consistent with a discontinuous canopy and exposed rock and soil. Interannual variability was small (SD 0.04, 0.06 and 0.05). All three indices peaked in 2023 (NDVI 0.242, SAVI 0.359, ARVI 0.169), the year with the highest temperature and lowest precipitation. A peak in the driest year is unlikely to indicate woody growth. Herbaceous or crop greening, composite selection and atmospheric contamination of the maximum-value composite could contribute, and none was tested.

The indices correlated strongly and positively with annual mean temperature (r = 0.969–0.996; Table 3) and negatively, but not significantly, with precipitation (r = −0.593 to −0.692). With five annual observations these coefficients are unstable, and temperature and greenness may simply share a trend over the period. They show association only and do not show that temperature controls greenness.

**Table 3: Pearson Correlations between Annual Mean Vegetation Indices and Annual Climate, Tula Highland, 2020–2024**

| Index | Climate variable | *n* | *r* | *p* | Remarks |
|---|---|---|---|---|---|
| ARVI | Precipitation | 5 | −0.593 | 0.292 | Not significant |
| ARVI | Temperature | 5 | 0.969 | 0.006 | Significant |
| NDVI | Precipitation | 5 | −0.687 | 0.201 | Not significant |
| NDVI | Temperature | 5 | 0.994 | 0.001 | Significant |
| SAVI | Precipitation | 5 | −0.692 | 0.195 | Not significant |
| SAVI | Temperature | 5 | 0.996 | < 0.001 | Significant |

n, number of years. Source: Landsat 8 analysis and climate data.

Correlations between raster-predicted AGB and the three indices exceeded 0.90 in every year (NDVI and SAVI 0.9405–0.9589; ARVI 0.9038–0.9191; 20,000 randomly sampled pixels per year). These values are expected, because predicted AGB is a linear function of the same indices, and they give no independent evidence of model validity. NDVI and SAVI correlations were identical to four decimal places in every year, which shows that the two indices are almost perfectly collinear.

**Model Performance and Selection**

Twenty-one models were fitted (Table 4). For untransformed AGB, the three-index model had the lowest AIC (173.93) and the highest adjusted $R^2$ (0.986), followed by NDVI + SAVI (AIC 175.86; adjusted $R^2$ 0.982) and NDVI alone (AIC 191.53; adjusted $R^2$ 0.931). The ΔAIC between the first two models is 1.93, below the threshold of 2, so NDVI + SAVI has similar support; NDVI alone was clearly weaker (ΔAIC = 17.60). Inverse-transformed models explained the least variance (best adjusted $R^2$ 0.476), and log-transformed models were intermediate (best adjusted $R^2$ 0.834, for the three-index model). Rankings in Table 4 are given within each response form because AIC is not comparable across them. The result differs from the regional pattern reported for single-index models (Yuguda et al., 2026).

**Table 4: Fit Statistics of the Candidate Models for Plot AGB and its Transformations, Tula Highland**

| Response | Predictors | Adjusted $R^2$ | AIC | Rank within response |
|---|---|---|---|---|
| AGB | NDVI + SAVI + ARVI | 0.9857 | 173.93 | 1 |
| AGB | NDVI + SAVI | 0.9823 | 175.86 | 2 |
| AGB | NDVI | 0.9306 | 191.53 | 3 |
| AGB | NDVI + ARVI | 0.9276 | 192.77 | 4 |
| AGB | ARVI | 0.8749 | 198.60 | 5 |
| AGB | SAVI + ARVI | 0.8610 | 200.60 | 6 |
| AGB | SAVI | 0.8513 | 200.67 | 7 |
| Log AGB | NDVI + SAVI + ARVI | 0.8336 | 31.66 | 1 |
| Log AGB | SAVI + ARVI | 0.8075 | 32.82 | 2 |
| Log AGB | NDVI + SAVI | 0.7914 | 33.78 | 3 |
| Log AGB | SAVI | 0.7419 | 35.60 | 4 |
| Log AGB | NDVI | 0.6640 | 38.77 | 5 |
| Log AGB | ARVI | 0.6410 | 39.56 | 6 |
| Log AGB | NDVI + ARVI | 0.6266 | 40.77 | 7 |
| Inverse AGB | SAVI + ARVI | 0.4704 | −62.48 | 1 |
| Inverse AGB | NDVI + SAVI + ARVI | 0.4761 | −62.02 | 2 |
| Inverse AGB | NDVI + SAVI | 0.3397 | −59.83 | 3 |
| Inverse AGB | SAVI | 0.2817 | −59.56 | 4 |
| Inverse AGB | NDVI | 0.2197 | −58.56 | 5 |
| Inverse AGB | ARVI | 0.1846 | −58.04 | 6 |
| Inverse AGB | NDVI + ARVI | 0.1514 | −56.82 | 7 |

Statistics refer to the calibration plots. Source: field survey (2025) and Landsat 8 analysis.

The selected equation (Table 5) has large coefficients of opposite sign for NDVI (+106,527) and SAVI (−63,095). This is typical of collinear predictors: the individual coefficients are unstable and cannot be read as separate effects of each index. The gain from NDVI alone (adjusted $R^2$ 0.931) to the three-index model (0.986) comes from small differences between nearly collinear predictors on 13 plots and may reflect noise as much as added information. The three-index model should not be regarded as superior until cross-validation supports it. Complementary information from the three indices, as suggested for heterogeneous terrain (Chen et al., 2025; Muhammad et al., 2024; Zhang et al., 2023), was not demonstrated here.

**Table 5: Selected Vegetation-Index Model for AGB, Tula Highland**

| Response | Predictors | Equation | Adjusted $R^2$ | AIC | Simulation CV (%) |
|---|---|---|---|---|---|
| AGB | NDVI + SAVI + ARVI | AGB = −2,556.13 + 106,527.47 × NDVI − 63,095.02 × SAVI + 14,609.84 × ARVI | 0.986 | 173.93 | 3.32 |

Adjusted $R^2$ and AIC refer to the calibration plots. Source: field survey (2025) and Landsat 8 analysis.

**Table 6: Monte Carlo Summary (500 Runs) for the Untransformed AGB Models, Tula Highland**

| Predictors | Mean simulated AGB | SD | Lower 95% | Upper 95% | CV (%) |
|---|---|---|---|---|---|
| NDVI | 2,384.46 | 174.01 | 2,050.42 | 2,719.55 | 7.30 |
| SAVI | 2,390.93 | 254.54 | 1,896.54 | 2,878.22 | 10.65 |
| ARVI | 2,402.38 | 238.65 | 1,939.99 | 2,868.34 | 9.93 |
| NDVI + SAVI | 2,387.26 | 85.79 | 2,218.23 | 2,556.58 | 3.59 |
| NDVI + ARVI | 2,384.57 | 172.51 | 2,041.43 | 2,710.97 | 7.23 |
| SAVI + ARVI | 2,396.75 | 241.56 | 1,920.73 | 2,871.51 | 10.08 |
| NDVI + SAVI + ARVI | 2,389.78 | 79.38 | 2,235.51 | 2,548.47 | 3.32 |

Values in kg $ha^{-1}$. Source: Monte Carlo analysis.

The three-index model had the lowest simulation CV (3.32%; Table 6). This CV shows that predictions are stable under the simulated input variation. It does not show that predictions are accurate, and a model fitted closely to 13 plots can be stable and still biased out of sample. Log-transformed models had CVs of 21.7–32.6%. Inverse-transformed models had CVs above 1,000% and 95% intervals that included negative biomass, and they were unsuitable for prediction, although

inverse transformation performs well in some studies (Poudel et al., 2023). Model selection should therefore consider stability and plausibility in addition to AIC and adjusted $R^2$.

**Validation**

Fit statistics describe agreement with the calibration plots and are not measures of predictive accuracy. With 13 plots and three correlated predictors, overfitting is likely. Individual plots strongly influence the fit; TH 12 alone holds 28% of the summed AGB and should be tested as an influential observation. Residual plots (Figure 2) show no obvious fan-shaped pattern, but with this sample they have little power to detect departures from constant variance.

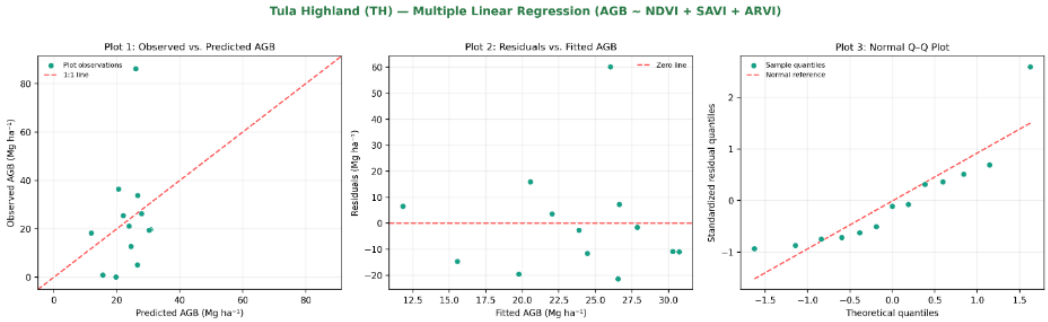



Figure 2: Diagnostic plots for the NDVI + SAVI + ARVI regression: observed against predicted AGB, residuals against fitted values, and normal Q–Q plot of residuals

Biomass in these plots is positively skewed, with two near-zero plots and one very large plot, yet untransformed AGB fitted better than the transformed forms. With only 13 plots this may reflect limited sampling rather than a true site characteristic. Stratifying the highland by rock cover and fitting separate relationships for open-rock and wooded areas would probably give more transferable models.

**Spatial and Interannual Patterns of Predicted AGB**

Applying the selected equation to the annual composites gave mean AGB of 1,963.65 kg ha$^{-1}$ in 2020 and 2,297.29 kg ha$^{-1}$ in 2024, an increase of 333.64 kg ha$^{-1}$ (16.99%; Figure 3). Annual means ranged from 1,680.85 to 3,142.49 kg ha$^{-1}$ (mean 2,169.27; SD 590.45; CV 0.272). Interannual variation was therefore larger than the 2020–2024 difference, and the highest annual mean coincided with the anomalous 2023 index peak. The change between two endpoint years is sensitive to the years chosen, and no trend test was applied to the five annual values.

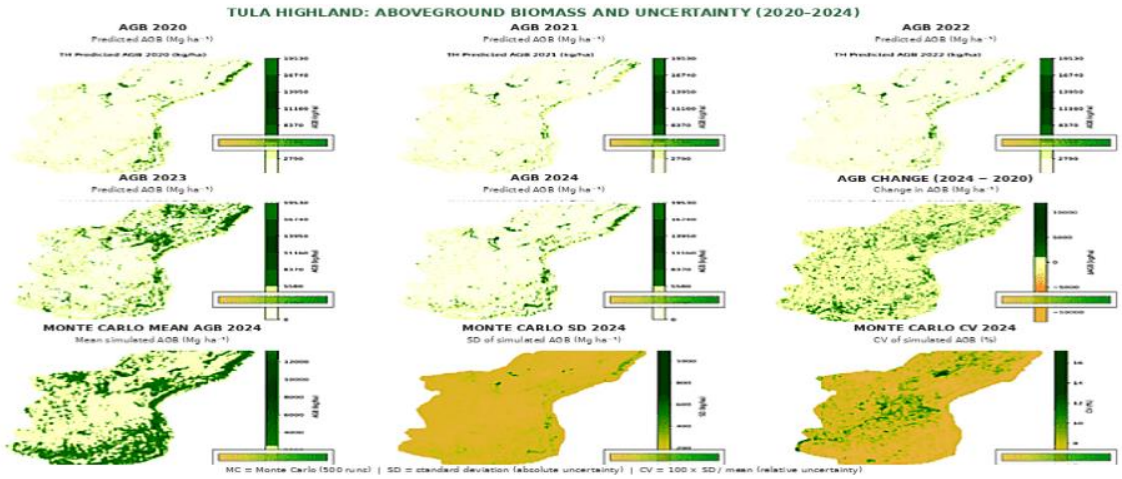



Figure 3: Predicted AGB (kg ha$^{-1}$) in Tula Highland for 2020–2024, change between 2020 and 2024, and the Monte Carlo mean, standard deviation and CV for 2024

An increase of this kind can arise from woody regeneration, from phenological or herbaceous variation, or from land-use change such as a shift from cropping to fallow or tree-based systems (Biah et al., 2023; Wang et al., 2024). The high interannual CV and the peak in the driest year suggest that at least part of the signal is not woody growth. Confirming durable biomass change requires repeated field inventories, or structural data from very-high-resolution imagery or LiDAR. The result is therefore reported as a model-derived spectral pattern. It is not evidence of carbon sequestration, and no projection beyond 2024 is made.

**Limitations**

The 13 plots cover about 0.2% of the highland and vary widely (CV 93%). Plots were placed systematically and not stratified by rock cover, so the mean may not represent the whole area. The allometric equations were developed in other regions and may not suit *Raphia sudanica*, a palm. BGB follows from a fixed ratio, and litter and soil carbon are excluded from the totals. Plot-to-pixel matching is imprecise, because each plot covers about 11 Landsat pixels, many of them mixed rock and vegetation, and top-of-atmosphere reflectance with dark object subtraction is less robust than surface-reflectance products. Finally, the field data come

from one year (2025) and the imagery precedes it, so image-based change cannot be validated.

**Conclusion**

Field inventory of 13 one-hectare plots in Tula Highland showed large spatial variation in aboveground and belowground biomass. Mean densities were 23.55 Mg ha$^{-1}$ aboveground and 6.12 Mg ha$^{-1}$ belowground (combined 29.67 Mg ha$^{-1}$, or 13.95 Mg C ha$^{-1}$), and the summed values across the plots were 306.14 and 79.60 Mg. A regression on NDVI, SAVI and ARVI fitted the calibration plots closely (adjusted $R^2$ = 0.986), but the small sample, collinear predictors and limited independent validation constrain confidence in spatial predictions. The 2020–2024 changes in Landsat-derived AGB are preliminary model-derived patterns and not confirmed carbon sequestration. More field plots, repeated inventories and a formal uncertainty assessment are needed before the model can support carbon accounting.

**REFERENCES**

Ajayi, O. L. P. (2026). Operationalisation of the Nigerian carbon market. Olaniwun Ajayi Insights. https://www.olaniwunajayi.net/blog/operationalisation-of-the-nigerian-carbon-market/

Asrat, Z., Taddese, H., Ørka, H. O., Gobakken, T., Burud, I., & Næsset, E. (2018). Estimation of forest area and canopy cover based on visual interpretation of satellite images in Ethiopia. Land, 7(3), Article 92.

Biah, I., Azihou, A. F., Guendehou, S., & Sinsin, B. (2024). Land use/land cover change and carbon footprint in tropical ecosystems in Benin, West Africa. Trees, Forests and People, 15, Article 100488.

Bordoloi, R., Das, B., Tripathi, O. P., Sahoo, U. K., Nath, A. J., Deb, S., Devi, N. B., & Gupta, A. (2021). Satellite data derived spatiotemporal variation of biomass carbon stocks and their relation with vegetation type in tropical forests of Assam in northeast India. Ecological Indicators, 123, Article 107341. https://doi.org/10.1016/j.ecolind.2021.107341

Bos, A. B., De Sy, V., Duchelle, A. E., Herold, M., & Martius, C. (2019). Global data and tools for local forest cover loss and REDD+ performance assessment: Gaps, needs and possible approaches. Environmental Science & Policy, 92, 357–367.

Burnham, K. P., & Anderson, D. R. (2002). Model selection and multimodel inference: A practical information-theoretic approach (2nd ed.). Springer.

Chabi, A., Lautenbach, S., Tondoh, J. E., Orekan, V. O. A., Kyei-Baffour, N., & Blaes, X. (2016). The relevance of using in situ carbon stocks and satellite indices to assess aboveground carbon stock of tropical forest ecosystems. iForest, 9, 606–615.

Chave, J., Condit, R., Aguilar, S., Hernandez, A., Lao, S., & Perez, R. (2004). Error propagation and scaling for tropical forest biomass estimates. Philosophical Transactions of the Royal Society B: Biological Sciences, 359(1443), 409–420.

Chave, J., Réjou-Méchain, M., Búrquez, A., Chidumayo, E., Colgan, M. S., Delitti, W. B. C., Duque, A., Eid, T., Fearnside, P. M., Goodman, R. C., Henry, M., Martínez-Yrízar, A., Mugasha, W. A., Muller-Landau, H. C., Mencuccini, M., Nelson, B. W., Ngomanda, A., Nogueira, E. M., Ortiz-Malavassi, E., Vieilledent, G. (2014). Improved allometric models to estimate the aboveground biomass of tropical trees. Global Change Biology, 20(10), 3177–3190. https://doi.org/10.1111/gcb.12629

Chen, C., He, G., Fang, H., Shi, L., Zhuang, Y., Ding, Z., Guo, J., Yue, X., Yang, K., & Xi, W. (2025). A study on the remote sensing estimation and spatiotemporal distribution patterns of aboveground biomass in savanna grasslands of the Yuanmou dry-hot valley. Frontiers in Plant Science, 16, Article 1648539.

Conti, G., Enrico, L., Casanoves, F., & Díaz, S. (2019). Shrub biomass estimation in the semiarid Chaco forest: A contribution to the understanding of South American dryland carbon sinks. Journal of Arid Environments, 166, 51–60.

Global Climate Observing System. (2016). The global observing system for climate: Implementation needs (GCOS-200). World Meteorological Organization.

Henry, M., Tittonell, P., Manlay, R. J., Bernoux, M., Albrecht, A., & Vanlauwe, B. (2009). Biodiversity, carbon stocks and sequestration potential in aboveground biomass in smallholder farming systems of western Kenya. Agriculture, Ecosystems & Environment, 129(1–3), 238–252. https://doi.org/10.1016/j.agee.2008.09.006

Herold, M., Carter, S., Avitabile, V., Espejo, A. B., Jonckheere, I., Lucas, R., McRoberts, R. E., Næsset, E., Nightingale, J., Petersen, R., Reiche, J., Romijn, E., Rosenqvist, Å., Rozendaal, D. M. A., Seifert, F. M., Sanz, M. J., & De Sy, V. (2019). The role and need for space-based forest biomass-related measurements in environmental management and policy. Surveys in Geophysics, 40, 757–778. https://doi.org/10.1007/s10712-019-09510-6

Huete, A. R. (1988). A soil-adjusted vegetation index (SAVI). Remote Sensing of Environment, 25(3), 295–309. https://doi.org/10.1016/0034-4257(88)90106-X

Intergovernmental Panel on Climate Change. (2006). 2006 IPCC guidelines for national greenhouse gas inventories (H. S. Eggleston, L. Buendia, K. Miwa, T. Ngara, & K. Tanabe, Eds.). Institute for Global Environmental Strategies.

Intergovernmental Panel on Climate Change. (2019). 2019 refinement to the 2006 IPCC guidelines for national greenhouse gas inventories (E. Calvo Buendia, K. Tanabe, A. Kranjc, J. Baasansuren, M. Fukuda, S. Ngarize, A. Osako, Y. Pyrozhenko, P. Shermanau, & S. Federici, Eds.). IPCC.

Jimoh, A. I., Hussaini, H., Aliyu, J., Sadiq, F. K., & Kefas, P. K. (2022). Assessment of the impacts of toposequence on soil properties and quality in Tula, Gombe State, Nigeria. Agricultura Tropica et Subtropica, 55(1), 99–107.

Kaufman, Y. J., & Tanré, D. (1992). Atmospherically resistant vegetation index (ARVI) for EOS-MODIS. IEEE Transactions on Geoscience and Remote Sensing, 30(2), 261–270. https://doi.org/10.1109/36.134076

Kumar, L., & Mutanga, O. (2017). Remote sensing of above-ground biomass. Remote Sensing, 9(9), Article 935. https://doi.org/10.3390/rs9090935

Ma, H., Mo, L., Crowther, T. W., Maynard, D. S., van den Hoogen, J., Stocker, B. D., Terrer, C., & Zohner, C. M. (2021). The global distribution and environmental drivers of aboveground versus belowground plant biomass. Nature Ecology & Evolution, 5, 1110–1122. https://doi.org/10.1038/s41559-021-01485-1

Mokany, K., Raison, R. J., & Prokushkin, A. S. (2006). Critical analysis of root:shoot ratios in terrestrial biomes. Global Change Biology, 12(1), 84–96. https://doi.org/10.1111/j.1365-2486.2005.001043.x

Muhammad, B., Rehman, A. U., Mumtaz, F., Qun, Y., & Zhongkui, J. (2024). Estimation of above-ground biomass in dry temperate forests using Sentinel-2 data and random forest: A case study of the Swat area of Pakistan. Frontiers in Environmental Science, 12, Article 1448648.

Poudel, A., Shrestha, H. L., Mahat, N., Sharma, G., Aryal, S., Kalakheti, R., & Lamsal, B. (2023). Modeling and mapping of aboveground biomass and carbon stock using Sentinel-2 imagery in Chure region, Nepal. International Journal of Forestry Research, 2023, Article 5553957.

PwC. (2023). Nigeria's Climate Change Act: Implications for business and investment. PricewaterhouseCoopers Nigeria.

Ravindranath, N. H., & Ostwald, M. (2008). Carbon inventory methods: Handbook for greenhouse gas inventory, carbon mitigation and roundwood production projects. Springer.

Rouse, J. W., Haas, R. H., Schell, J. A., & Deering, D. W. (1974). Monitoring vegetation systems in the Great Plains with ERTS. In Proceedings of the Third Earth Resources Technology Satellite-1 Symposium (Vol. 1, pp. 309–317). NASA.

Rügnitz, M. T., Chacón, M. L., & Porro, R. (2009). Guía para la determinación de carbono en pequeñas propiedades rurales. ICRAF.

Temesgen, H., Affleck, D., Poudel, K., Gray, A., & Sessions, J. (2015). A review of the challenges and opportunities in estimating above ground forest biomass using tree-level models. Scandinavian Journal of Forest Research, 30(4), 326–335.

Tomlin, C. D. (1990). Geographic information systems and cartographic modeling. Prentice Hall.

Tucker, C. J. (1979). Red and photographic infrared linear combinations for monitoring vegetation. Remote Sensing of Environment, 8(2), 127–150. https://doi.org/10.1016/0034-4257(79)90013-0

Wang, M., Ciais, P., Fensholt, R., Brandt, M., Tao, S., Li, W., Fan, L., Frappart, F., Sun, R., Li, X., Liu, X., Wang, H., Cui, T., Xing, Z., Zhao, Z., & Wigneron, J.-P. (2024). Satellite observed aboveground carbon dynamics in Africa during 2003–2021. Remote Sensing of Environment, 301, Article 113927.

Yanai, R. D., Battles, J. J., Richardson, A. D., Blodgett, C. A., Wood, D. M., & Rastetter, E. B. (2010). Estimating uncertainty in ecosystem budget calculations. Ecosystems, 13, 239–248.

Yilangai, R. M., Abalaka, J., Nsor, C. A., Babale, A., Karau, S. D., & Ivande, S. (2023). Effect of disturbance on bird feeding guilds in a West African dry forest. African Journal of Ecology, 61(2), 461–468.

Yuguda, U. A., Saka, M. G., Dishan, E. E., Abba, H. M., & Bello, M. B. (2026). Spatial patterns and temporal dynamics of aboveground-belowground biomass and carbon stocks in Kanawa Forest Reserve, Gombe State, Nigeria. Bima Journal of Science and Technology, 10(3). https://doi.org/10.64290/bima.v10i3.1651

Zhang, Y., Liang, S., & Yang, L. (2019). A review of regional and global gridded forest biomass datasets. Remote Sensing, 11(23), Article 2744.

©2026 This is an Open Access article distributed under the terms of the Creative Commons Attribution 4.0 International license viewed via https://creativecommons.org/licenses/by/4.0/ which permits unrestricted use, distribution, and reproduction in any medium, provided the original work is cited appropriately.